The W-type W UMa Contact Binary MU Cancri

Andrew P. Odell *(deceased May 2019)*
Emeritus Associate Professor of Physics and Astronomy, Northern Arizona University, Flagstaff, AZ 86011

Joel A. Eaton
7050 Bakerville Road, Waverly, TN 37185; eatonjoel@yahoo.com

Abstract   We use three complete light curves for MU Cancri, a faint W-type W UMa contact binary, to investigate possible mechanisms for changes in such binaries' light curves. The standard Roche model, as implemented by the Wilson-Devinney code, does not fit the observations at their level of precision. Most of this discrepancy can be explained by placing one or two moderate starspots ($r_{spot} \sim 10$–12°) on the more massive component. However, this does not resolve the discrepancy, since the solutions for the three epochs have different mass ratios, implying unmodelled changes in eclipse depths. This, in turn, implies that more spots are changing the depths in unpredictable ways. Thus we are confronted with limits on just how precisely light curve solutions can define the physical properties of a contact binary. We use spectra to classify the star (G3–G7) and to measure a spectroscopic mass ratio (q = 2.63), significantly closer to 1.0 than the photometric mass ratios (3.0–3.3), but this difference is unlikely to be caused by third light. And we also extend the period study of Alton and Stępień.

1. Introduction

MU Cancri (GSC 01397-01030; TYC 1397-1030-1; NSVS 10133793; $V \approx 12.1$) is a faint contact binary discovered by Pepper *et al.* (2007). It came to our attention when Shanti Priya, Sriram, and Vivekananda Rao (2013) published a photometric study finding a mass ratio surprisingly large (close to unity) for such a star. Consequently, we have obtained complete light curves at three epochs in 2014 and 2016, another incomplete one in 2019, and spectra for measuring radial velocities in 2013. In the meantime Alton and Stępień (2018) have obtained a light curve, which they analyzed with the Wilson-Devinney model, and did a period analysis, finding periodic changes in the times of conjunction, presumably from an orbit with an unseen companion.

Contrary to Shanti Priya *et al.* (2013), we find that this star is a rather conventional W-type W UMa binary with some moderately small spots on its surface. We have analyzed the new light curves in three ways: 1) as a standard W UMa binary without spots, 2) with third light, and 3) with dark spots.

2. Observations

2.1. Photometry

We took new light curves of MU Cnc for three epochs, 2014 (16 Feb. and 17–18 March UT), 2016-February (17, 18, 24, and 28 February and 1 March UT), and 2016-November (14 and 15 Nov. UT), and a partial light curve for 24 April 2019. The first of these comes from Mt. Bigelow Observatory of the University of Arizona, the others from the robotic telescope ROBO at Lowell Observatory. Our photometry consists of differential magnitudes measured with the usual commercially available *BVRI* filters (Cousins *RI*); they are not transformed to the standard system via observations of standard stars. Since the variable and comparison stars were all on the same CCD images, we have not corrected them for differential extinction, either. The data are available from the AAVSO ftp archive as the ASCII file

MUCnc-JAAVSO-482.txt at ftp://ftp.aavso.org/public/datasets/. Listed are the Reduced Julian Date (RJD = HJD–2400000) of observation, and differential magnitudes of the variable and check stars for the four passbands. The datasets are identified by a symbol at the end of each line, namely, 2014, 2016-feb, 2016-nov, and 2019. Entries with missing data are identified with magnitudes equal to 99.999. There are roughly 250, 300, 140, and 75 data in each color, respectively, for the four epochs.

The standard deviations of the check-star observations for the *V* band, which indicate the precision of the data, were 0.016, 0.004, 0.003, and 0.004, respectively, for our four epochs, 2014–2019. Averages of the check star ΔVs for the last three epochs agreed to within ±0.001 mag.

Figure 1 shows the comparison stars we used at the two observatories. The comp star for 2014 was the average of the
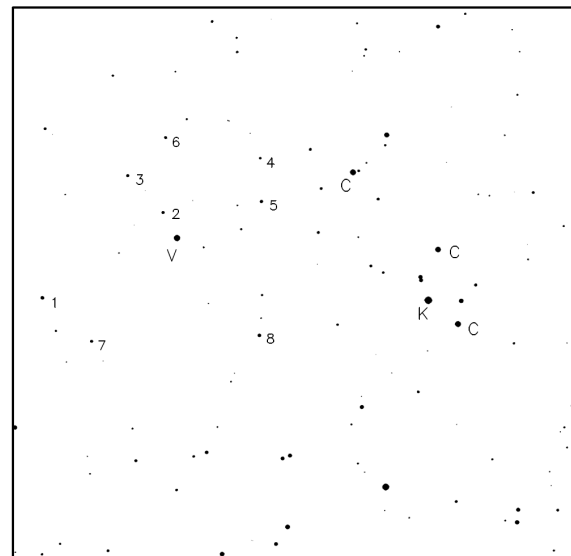

Figure 1. Comparison stars used. This is a 20×20 arcmin. field from the red Palomar Sky Survey. MU Cnc is marked with a V, the 8 comparisom stars used in 2014 with numbers, the 3 comparison and check stars for 2016 and 2019 with Cs and a K, respectively.

eight numbered stars. For the three later epochs, the comp was the average of the three stars labeled C, and K was the check star.

2.2. Spectroscopy

We also obtained 20 spectra for MU Cnc with the Meinel spectrograph at Steward Observatory in Dec. 2013 (Table 1), covering the wavelength range 4150–4900Å (0.71Å/pix, R~3500). These provide a spectral classification of the star and measurements of the radial velocities of both binary components.

To determine a spectral type, we compared spectra for the two conjunctions with spectra of some single stars artificially broadened to $v_{rot}\sin i = 150\,km\,s^{-1}$ used in a paper about W Crv (Eaton, Odell, and Nitschelm 2020). These were HD 38722 (F8), HD 50692 (G0 V), HD 42807 (G2 V), HD 31501 (G8 V), and HD 103095 (K1 V). MU Cnc is definitely later than G2 but earlier than G8 and is marginally later (cooler) at primary eclipse than at secondary eclipse. Given the standards available, we can only say the type is in the range G3–G7.

Odell derived the radial velocities by using IRAF to fit double Gaussians to cross-correlation functions. These are the velocities given in Table 1, where, following the photometric convention, Star 1 is the component eclipsed at primary minimum and Star 2 is the one eclipsed at secondary minimum. We have fit sine curves to them to derive the orbital elements $K_1 = 254 \pm 14\,km\,s^{-1}$, $K_2 = 102 \pm 4\,km\,s^{-1}$, and $\gamma = 21 \pm 3\,km\,s^{-1}$, for which the spectroscopic mass ratio is $q_{sp} = 2.50 \pm 0.46$. They are plotted with the data in Figure 2; you will notice that the lines representing the elements do not cross at phase zero. This is because γ is 13 km s^{-1} larger for the fainter star. This must result from a systematic error on one side of that star's orbit, likely near phase 0.25. That would mean K_1 should be increased by approximately this offset to give $K_1 \sim 267\,km\,s^{-1}$ and $q_{sp} \sim 2.63$. In any case, this spectroscopic mass ratio is significantly larger than the photometric mass ratio, which we will try to explain by invoking third light.

3. Ephemeris

Alton and Stępień (2018) analyzed the times of minimum, finding that they vary periodically, probably from the light-time effect in a triple system. To their seven newly determined times of minimum (ToMs), we have added 15 more from Mt. Bigelow and ROBO and have added 27 others we measured with published archival data, the latter coming from Harvard patrol plates, NSVS (Northern Sky Variability Survey; Wozniak *et al.* 2004), CSS (Catalina Sky Survey; Univ. Arizona 2006–2009), ASAS (All Sky Automated Survey; Pojmański 1997), and KELT (Kilodegree Extrememly Little Telescope; Pepper *et al.* 2007).

All these times of minimum are listed in Table 2. The sigmas in column 2 are estimated uncertainties, used for weighting (σ^{-2}) in the determination of light elements. The epochs listed in column 3 were carefully identified by Odell by extending the best apparent period at a given epoch backward in time. The (O–C)s in column 4 are with respect to the period found for recent data (Equation 2); the (O-C)s in column 5 come from fitting these residuals with a quadratic but with the data

Table 1. Radial velocities for MU Cnc.

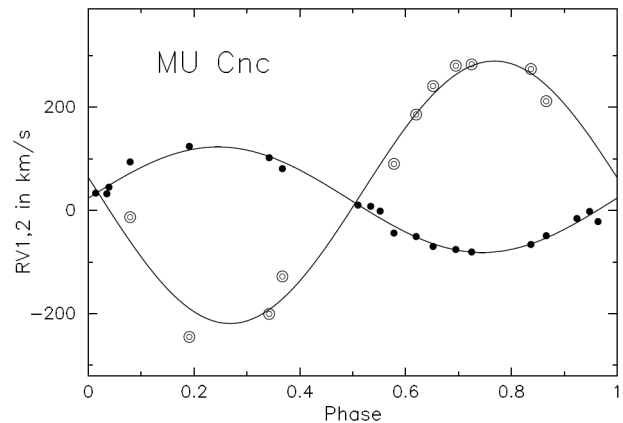| RJD	Phase	RV$_1$	RV$_2$
56636.8090	0.964	—	–21.7
56636.8234	0.014	—	33.4
56636.8308	0.039	—	44.9
56639.7396	0.035	—	32.0
56639.7526	0.079	–13.2	93.8
56639.7850	0.191	–245.2	123.9
56639.8291	0.342	–200.7	101.9
56639.8363	0.367	–128.0	80.8
56639.8781	0.510	—	10.1
56639.8851	0.534	—	7.8
56640.7633	0.552	—	–1.5
56640.7709	0.578	89.9	–44.0
56640.7831	0.620	185.6	–50.7
56640.7923	0.652	240.7	–70.0
56640.8049	0.695	280.2	–75.9
56640.8135	0.725	282.8	–80.7
56640.8462	0.837	273.8	–66.1
56640.8547	0.866	211.5	–49.1
56640.8715	0.924	—	–15.8
56640.8786	0.948	—	–2.1

Figure 2. Velocity curves for MU Cnc. Circles are for the photometric primary star (eclipsed at phase 0.0), dots for the brighter photometric secondary. Lines are the fitted sine curves for which $K_1 = 254$ and $K_2 = 102$ km s^{-1}.

unweighted (Equation 3). Column 6 gives the data archive and the year from which the time of minimum was obtained.

To determine a time of minimum (ToM), Odell entered the data (ΔMag vs. HJD) in a spreadsheet, which he used to plot them against themselves reflected about a trial ToM, adjusting the trial ToM to make the reflected light curve coincide with the direct light curve on the plot. He estimated an uncertainty of 0.5–1 min. for continuous photometry. For the archival data, we estimate uncertainties of 0.01 d. for Harvard, 0.003 for ASAS, 0.005 for CSS, 0.003 for NSVS, and 0.0015 for KELT. For determinations taken from the literature, we have tried to use the published values but have set a minimum uncertainty of 0.0003 d., feeling that smaller values are unrealistic and wanting to avoid having such values bias our analysis of period changes.

Figure 3 shows the timings for a period determined for modern data, roughly RJD > 50,000. For earlier (Harvard) data the period seems to be much shorter, giving the following two piece-wise linear relationships:

$$HJD\,(Obs) = 4553526.379(8) + 0.2910074(1)\,\phi,$$
$$\text{for RJD} < 50,000, \qquad (1)$$

Table 2. Times of minimum light.

RJD	σ (d)	Epoch	(O–C)₁	(O–C)₂	Source*
22082.475	0.01	–108052.0	0.6045	–0.0321	Harvard-1919
23516.863	0.01	–103123.0	0.5867	–0.0002	Harvard-1923
28603.6150	0.01	–85643.0	0.4219	–0.0051	Harvard-1937
29585.7900	0.01	–82268.0	0.4261	0.0271	Harvard-1939
32262.6150	0.01	–73069.5	0.3630	0.0354	Harvard-1947
43131.8740	0.01	–35719.0	0.1204	0.0110	Harvard-1976
44308.7200	0.01	–31675.0	0.1076	0.0149	Harvard-1980
46095.7950	0.01	–25534.0	0.0684	–0.0015	Harvard-1985
47200.9000	0.01	–21736.5	0.0494	–0.0080	Harvard-1988
51554.7130	0.0030	–6775.5	0.0087	–0.0109	NSVS-2000
52622.8630	0.0005	–3105.0	–0.0065	–0.0197	Pilecki and Stępień (2012)
52727.7750	0.0030	–2744.5	–0.0049	–0.0176	ASAS-2003
53036.8320	0.0030	–1682.5	–0.0043	–0.0153	ASAS-2004
53432.7584	0.0015	–322.0	–0.0018	–0.0109	KELT-2005
53432.9054	0.0015	–321.5	–0.0003	–0.0094	KELT-2005
53474.6641	0.0015	–178.0	–0.0021	–0.0110	KELT-2005
53475.6840	0.0015	–174.5	–0.0007	–0.0096	KELT-2005
53526.4680	0.0030	0.0	0.0014	–0.0072	NSVS-2000
53702.8257	0.0030	606.0	0.0049	–0.0029	NSVS-2000
53853.5680	0.0030	1124.0	0.0022	–0.0050	NSVS-2000
53874.6611	0.0050	1196.5	–0.0032	–0.0103	CSS-2006
54194.6394	0.0050	2296.0	0.0057	–0.0001	—
54066.8890	0.0050	1857.0	0.0102	0.0040	CSS-2007
54479.6860	0.0050	3275.5	0.0045	–0.0002	CSS-2008
54905.7275	0.0050	4739.5	0.0022	–0.0010	CSS-2009
55290.7349	0.0003	6062.5	–0.0013	–0.0034	Diethelm (2010)
55555.8430	0.0050	6973.5	–0.0066	–0.0079	CSS-2011
55572.8704	0.0003	7032.0	–0.0035	–0.0047	Diethelm (2011)
55667.7409	0.0003	7358.0	–0.0034	–0.0044	Diethelm (2011)
55668.3223	0.0020	7360.0	–0.0040	–0.0050	28SC+ST7XME
55669.3402	0.0020	7363.5	–0.0047	–0.0057	28SC+ST7XME
55932.8517	0.0003	8269.0	–0.0059	–0.0063	Diethelm (2012)
55932.9996	0.0004	8269.5	–0.0036	–0.0039	Diethelm (2012)
55984.3678	0.0010	8446.0	0.0008	0.0005	Rukmini and Shanti Priya (2016)
56704.7696	0.0005	10921.5	–0.0015	–0.0004	Bigelow-2014
56733.7267	0.0005	11021.0	–0.0002	0.0009	Bigelow-2014
56733.8732	0.0005	11021.5	0.0008	0.0019	Bigelow-2014
56734.5997	0.0005	11024.0	–0.0003	0.0009	Bigelow-2014
56734.7469	0.0005	11024.5	0.0014	0.0026	Bigelow-2014
56734.8925	0.0005	11025.0	0.0015	0.0027	Bigelow-2014
56792.6577	0.0005	11223.5	0.0005	0.0018	Bigelow-2014
57435.8048	0.0005	13433.5	0.0077	0.0096	ROBO-2016
57442.6434	0.0005	13457.0	0.0075	0.0094	ROBO-2016
57442.9344	0.0005	13458.0	0.0074	0.0094	ROBO-2016
57446.8636	0.0005	13471.5	0.0080	0.0099	ROBO-2016
57448.9006	0.0005	13478.5	0.0079	0.0098	ROBO-2016
57454.5746	0.0003	13498.0	0.0071	0.0091	Alton and Stępień (2018)
57455.5936	0.0003	13501.5	0.0076	0.0095	Alton and Stępień (2018)
57456.6118	0.0003	13505.0	0.0072	0.0092	Alton and Stępień (2018)
57469.5617	0.0003	13549.5	0.0070	0.0090	Alton and Stępień (2018)
57471.5995	0.0003	13556.5	0.0077	0.0097	Alton and Stępień (2018)
57484.5498	0.0003	13601.0	0.0079	0.0099	Alton and Stępień (2018)
57495.6085	0.0003	13639.0	0.0081	0.0101	Alton and Stępień (2018)
57706.8808	0.0005	14365.0	0.0046	0.0067	ROBO-2016
57707.8995	0.0005	14368.5	0.0047	0.0069	ROBO-2016
57788.2161	0.0005	14644.5	0.0016	0.0038	Nagai (2018)
57788.3610	0.0005	14645.0	0.0010	0.0032	Nagai (2018)
58159.1059	0.0005	15919.0	–0.0054	–0.0031	Nagai (2019)
58443.1321	0.0005	16895.0	–0.0084	–0.0061	Nagai (2019)
58597.8020	0.0005	17426.5	–0.0122	–0.0100	ROBO-2019

*Source is the data archive and the year from which the time of minimum was obtained.

Table 3. MU Cnc: light curve solutions.

Parameter	No Spots or L3	L3, No Spots	Spots, 2014	Spots, 2016-Feb.	Spots, 2016-Nov.	Alton and Stępień (2018)
i (°)	80.4(3)	80.40 (fixed)	79.6(3)	79.9(2)	79.1(3)	81.35
q (M_2 / M_1)	3.089(11)	2.63 (fixed)	3.026(26)	3.090(3)	3.295(13)	2.825
ω	6.651(18)	5.995(10)	6.542(36)	6.669(9)	6.945(17)	6.283
fillout	12.3 ± 1.7%	20.5 ± 1.5%	17.6%	10.7%	9.7%	16.4%
T_1 (K, fixed)	5600	5600	5600	5600	5600	5807
T_2 (K)	5451(70)	5422(110)	5493(17)	5550(27)	5508(27)	5620
$<\sigma_{fit}>$	0.0049	0.0056	0.0059	0.0026	0.0017	
				$\ell 3/(\ell_1 + \ell_2)$		
B	—	0.079	—	—	—	0.064
V	—	0.068	—	—	—	0.073
R_c	—	0.075	—	—	—	—
I_c	—	0.094	—	—	—	0.558
			Spots on the More Massive Component			
long (°)	none	none	49(10)	159(5) and 328(4)	146(3)	none
rspot (°)	—	—	10.8(8)	12.3(11) and 11.0(7)	14(1)	—

Note: Numbers in parentheses are the errors of the last digits. All spots are assumed to be on the equator and to have a temperature 80% of the underlying photosphere.

and

$$HJD(Obs) = 4553526.4666(14) + 0.29101355(14)\phi,$$
$$\text{for } RJD > 50000, \quad (2)$$

numbers in parentheses being uncertainties of the last digits, φ being the phase. These fits are shown in the top panel of Figure 3.

We have also fit the linear residuals with a quadratic equation, weighting the data equally, to give the following quadratic elements:

$$HJD(Obs) = 4553526.4752(4) + 0.2910122(1)\phi + 4.1(1) \times 10^{-11}\phi^2. \quad (3)$$

This quadratic fit is not very convincing, and a quadratic fit calculated with realistic weights simply failed to fit the data.

It's disturbing that we have found an abrupt period increase at just the break between the ToMs from Harvard patrol plates and modern measurements; obviously one should be skeptical of this result. Yet the light curves seem to be reasonable, and Odell's extension of the phases did not break on close inspection [JAE]. Also, there have been precipitate period changes in other contact binaries (e.g. Pribulla *et al.* 1997).

The residuals from Eqation 2 are clearly cyclic as discovered by Alton and Stępień. These are shown in the lower panel of Figure 3. The period seems to be in the range 2930 ± 100 d. Fitting a sine curve to these residuals (Equation 4), we derive a semiamplitude of 9.2 min, corresponding to an orbit with $a_{1,2} \sin i = 1.10$ au for a light-time effect.

$$(O–C) = 0.0064(5) \sin(2\pi(RJD - 50,712)/2930) \quad (4)$$

The variation expected in the γ velocity of the eclipsing system would then be ±4 km s⁻¹ over 8 years. There is obviously more here than motion in a wide orbit, since the last three points in the lower panel of Figure 3 depart considerably from the fitted curve.
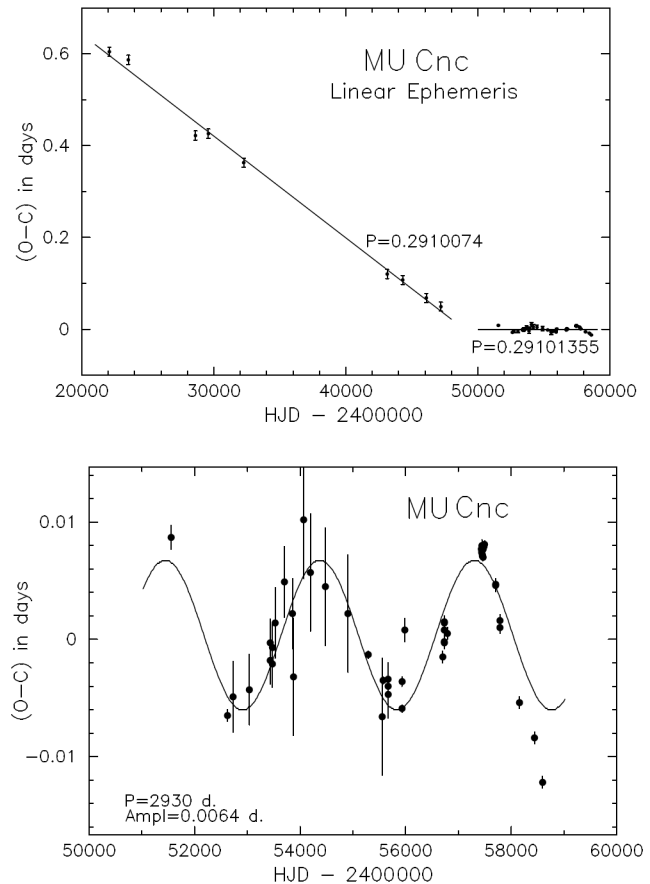

Figure 3. (O–C) diagrams for MU Cnc. Upper: Piece-wise linear ephemerides for residuals with respect to Equation 2. Lower: Periodic deviations from the linear fit for modern data (Equation 2). The sinusoid is the fit of Equation 4.

4. Light curve solutions

Our three complete light curves give us the opportunity to look at changes in the light curve and their possible causes.

Some elements cannot change materially over a period of a few years, so they have to be the same for all three of our epochs. These include the total mass $M_1 + M_2$, the mass ratio, q, the inclination, i, third light, and—likely—the total luminosity of the system. Others might well change, such as spottedness from random variation in magnetism, and both the degree of fillout (Ω) and the temperature difference ($T_1 - T_2$), should the energy-transfer mechanism change, perhaps through magnetic modulation.

We have solved our light curves with the Wilson-Devinney code (WD 2015 version; see Wilson and Devinney (1971); Wilson (1990, 1994); Wilson and van Hamme (2015)), finding the elements in Table 3. These are roughly consistent with Alton and Stępień's solution (see Table 3, column 7). In these calculations we adopted a temperature of the primary consistent with its spectral class, convective gravity darkening (Lucy 1967), convective reflection effect (Ruciński 1969), the Kurucz-atmospheres option in the WD code, and linear limb-darkening coefficients from van Hamme (1993) calculated by the WD code. The σ_{fit}s listed are the median weighted residuals calculated by the WD code. The quoted errors of the elements are the standard deviations of the three solutions for columns 2 and 3, and the standard errors from the WD code, multiplied by 3 per Popper (1984) for the others. Calculated fits are shown in Figures 4 through 8.

We also included both velocity curves in the solution for the cases having no spots but omitted the velocities of the less massive star for the analyses with spots.

4.1. No third light, no spots

This represents the traditional approach to contact binaries. We started by solving the three light curves separately to see just how much variation in the elements to expect. For the principal elements, the range was 0.005 in Ω (potential of the surface), 0.012 in q, 0.42° in i, and 189 K in T_2. We then picked roughly average values for those element not expected to vary and solved the light curves again to detect changes in the potentially more volatile elements. Results are given in column 2 of Table 3, a plot of the fit for 2016-feb, our most extensive data set, in Figure 4. With the mass ratio fixed, Ω increased by 0.037 from 2014 to 2016-nov, with fillout decreasing from 15% to 9%, and T2 falling by 144 K.

4.2. Third light?

The marked difference between the mass ratios determined photometrically and spectroscopically suggests that the putative third star giving the light-time effect seen in Figure 3 is also contributing a measurable amount of third light. To test this idea, we solved the light curves again with the mass ratio fixed at the spectroscopic value (2.63). Results are given in column 3 of Table 3 and plotted for 2016-feb in Figure 5. Although the mean residuals we found are slightly smaller than for the solution without third light, this result is not convincing physically. The third light derived varied by a factor of about 3–4 amongst our three light curves when we solved them individually, and the average value we give in Table 3 has a spectrum much too like the eclipsing pair (too early) to be light from a dwarf companion, as did the spectrum of ℓ_3 in the separate solutions.

4.3. Minimal spots

This system is a W-type contact binary with the cooler, more massive component eclipsing its companion at primary minimum. That is obvious from the velocity curves in Figure 2, but it also follows from the shapes of the eclipses. Such systems have long been suspected of being heavily spotted. In fact, a different level of uniform spottedness between the components has even been suggested as the cause of their apparent temperature difference (e.g. Eaton *et al.* 1980; Eaton 1986; Barnes *et al.* 2004; Stępień 2009). Barnes *et al.* found evidence in their wonderful Doppler images of AE Phe that both components of that star are highly spotted, finding convincing trails of some individual spots in their line profiles and arguing somewhat less convincingly for evidence of *many* more small spots. So we wonder what effect spots have on this system.

Even a cursory inspection of Figures 4 and 5 shows that the model does not really fit the data at the level of their precision. Such deviations are usually explained by invoking spots, often a rather surprising number of them (e. g. Samec *et al.* 2010) and in bizarre locations (e. g. Samec *et al.* 2011). We have looked at the question of just how few spots we would need to explain these deviations. And we have also decided to place the spots only on the larger, more massive star, if possible. Obviously there could be spots on both stars, as Barnes *et al.* (2004) found for AE Phe. Furthermore, from our experience with RS CVn binaries we do not think the WD model is good enough to measure spot latitudes, so we place the spots on the equator. Latitude can be quite difficult to determine, even with top-of-the-line Doppler images (see Barnes *et al.* 2004, section 4).

We'll start with a spot solution for 2016-nov. The light curve here lies below the calculations on the rising branch of primary minimum, and a single moderate spot improves the fit markedly (Table 3, column 6 and Figure 6).

The light curves for 2014 and 2016-feb are both more complicated, 2014 showing an approximate classical O'Connell effect, with phases near 0.25 noticeably depressed. At this epoch, we started with a single spot to remove this depression. (Table 3, column 4 and Figure 7), although not at the longitude we had expected. There are likely more spots for 2014, but the data are not precise enough to justify looking further.

The light curves for 2016-feb showed the rising branches of both eclipses depressed, requiring two spots. These we placed on the cooler component, although they could have been on either. However, there may be some distortion of secondary minimum by the eclipse of the spot at longitude 328° that settles the ambiguity for that spot (Figure 8).

We again set the stable parameters to average values for the three solutions (i = 79.51° and q = 3.180) and solved the light curves a second time. The mean residuals increased a meaningless 7–18%, the spots remained roughly the same, but the fillout dropped from ~ 18% from the first two epochs to 6% for 2016-nov.

The big question here is whether changes in spots can account for the apparent variation in such physical quantities as Ω and $T_1 - T_2$. In our analysis of the three epochs, it did not. The variation of the derived inclination remains above the uncertainties of measurement, but the unexpected variation
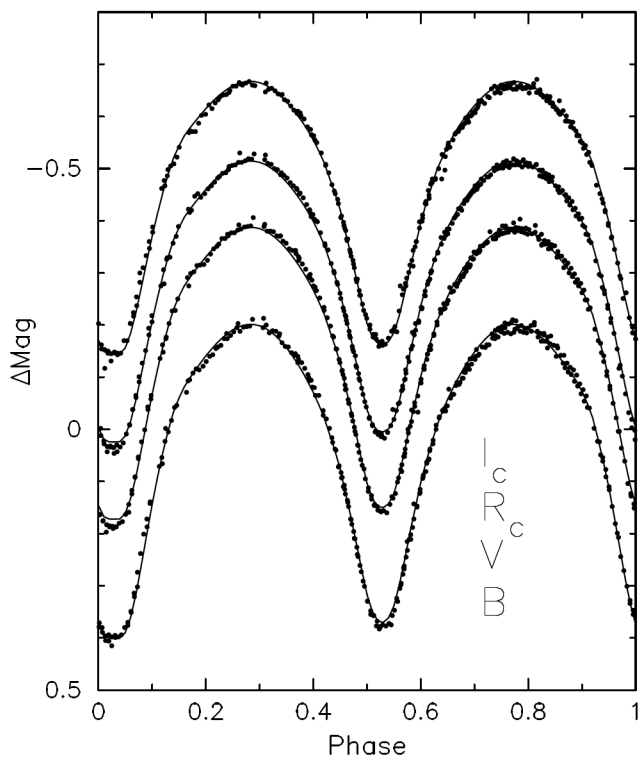
Figure 4. Light curve fit for February 2016 with no third light or spots. Notice how the fitted curve lies above the observations on both rising branches (φ ~ 0.2 and 0.7) and below on the falling branch of secondary eclipse.
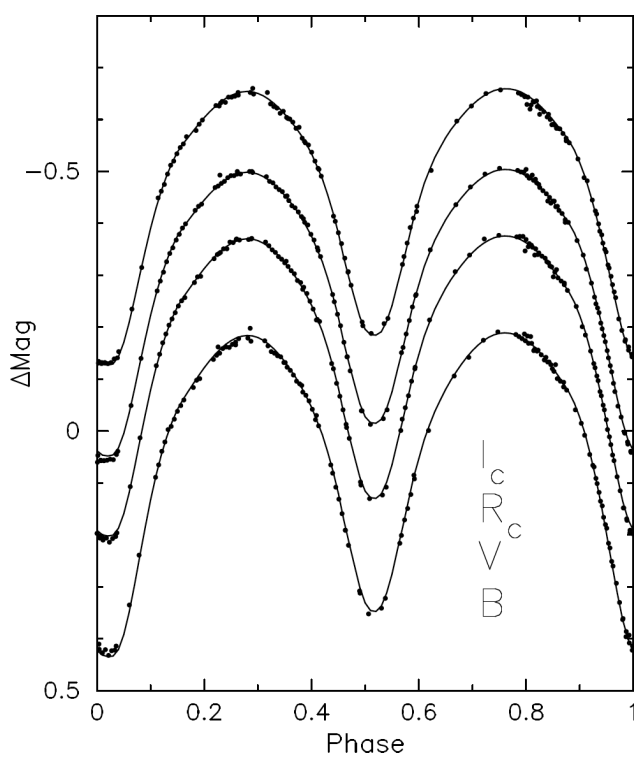

Figure 6. Light curve fit for 2016-nov with one dark starspot on the larger component.
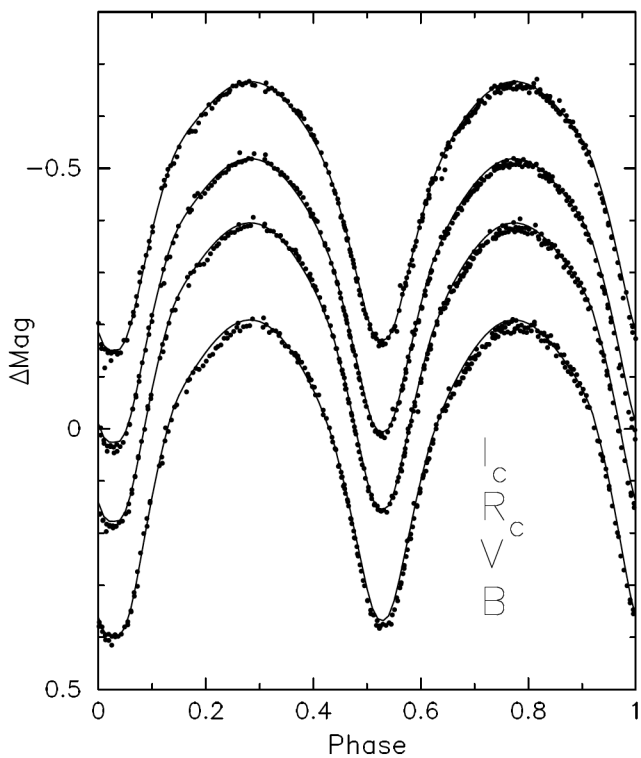

Figure 5. Light curve fit for February 2016 with third light. We fix the mass ratio at its spectroscopic value, fit the light curves, and derive the third light for the four passbands.

Figure 7. Light curve fit for 2014 with a dark starspot on the larger component.
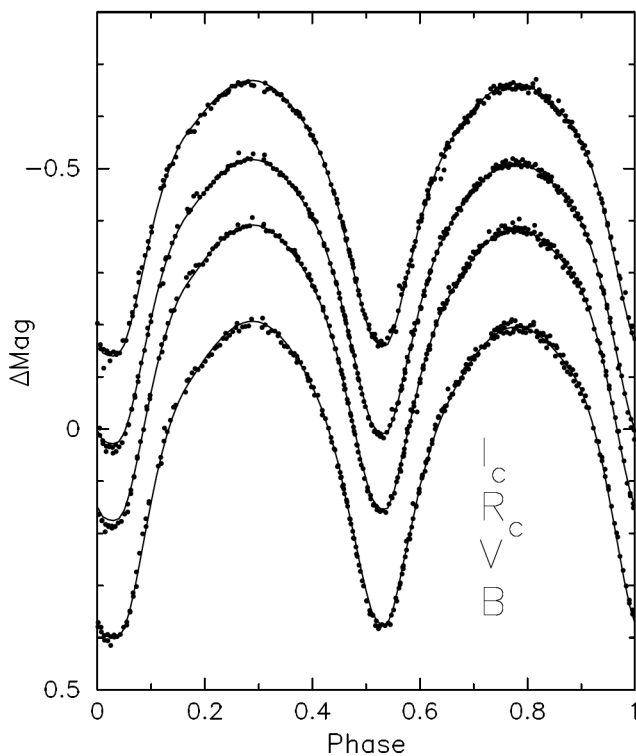
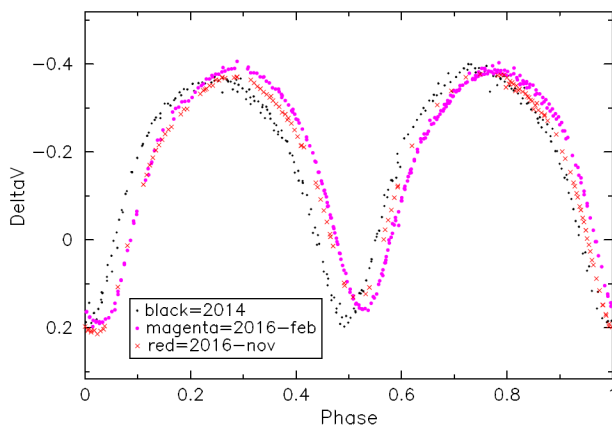Figure 8. Light curve fit for 2016-feb with two dark starspots on the larger component.

Figure 9. A comparison of the levels and shapes of the light curves at the three epochs. Symbols: small black dots = 2014, large magenta dots = 2016-feb, and red xs = 2016-nov.

of the mass ratio is completely perverse. Here, we are back to the question of whether spottedness is the cause of the W-type phenomenon. We will not address that possibility at this time, if merely to reflect Odell's extreme skepticism of light curve solutions featuring large numbers of apparently arbitrarily located spots. However, if a changing distribution of spots is not the cause of the changing depth of the eclipses, then some *unknown* mechanism must be responsible.

5. Discussion

We have complete light curves for three epochs, two of which were taken with the same instrument. The small

magnitude differences between the comp and check stars for those two latter epochs show that the photometric system was quite stable and that the comparison stars did not vary. Thus we would expect any changes between these light curves to be caused by the star itself, not by changes in the photometric system. Furthermore, since this star has marginally total eclipses, the light curve solutions should be fairly reliable.

Including third light did not explain the discrepancy between photometric and spectroscopic mass ratios. Most likely that results from systematic errors in the velocities of fainter component. The main effects of third light on the solution are to give a larger mass ratio (closer to 1.0) and a thicker common envelope. Indeed, the solution from Alton and Stępień—itself with third light—shows both effects, giving a derived mass ratio and larger filling factor consistent with our values.

Dark starspots certainly can explain some of the more obvious deviations of the star from the Roche model. However, including only one or two such spots did not resolve the problem of changes of q, i, and Ω amongst the light curves. At this time, that would seem to imply a much more extensive distribution of dark spots, one that really does not change greatly with time. This would make the cool contact binaries different from the RS CVn binaries, which show much larger apparent concentrations of spots with putative magnetic cycles. We do not think these latter phenomena are seen in W UMa binaries, but the data that would reveal them are rather scanty (but see Ruciński and Paczynski (2002) for a cautionary tale). A further point in favor of much more extensive spottedness is a variation in the general levels of the light curves. Figure 9, a plot of the *V* light curve for the three epochs, shows that the level at both maxima changed, despite our expecting the star to have a constant brightness beyond the slight depressions modelled with a few discrete spots.

Envelope circulation in these contact binaries must have significant effects on their magnetism, at least in its distribution. The W UMa systems are fairly strong sources of chromospheric/transition-region emission with high levels of X-ray flux, roughly covered uniformly with active regions (Ruciński and Vilhu 1983; Ruciński *et al.* 1985; Stępień *et al.* 2001; Chen *et al.* 2006), which means they are almost certainly highly magnetic. The apparent lack of large concentrations of spots in contact systems may reflect the inability of spots to stick around long enough to develop large structures. Also, such concentrations are readily explained by a random distribution of such spots, but only if the spots are moderately large and not too numerous (Eaton *et al.* 1996). As the spots become smaller and more numerous, the effect of random clumping declines.

Spots, at least in the Sun, seem to be a superficial phenomenon not anchored deeply in the star—somewhat like Jupiter's Red Spot and analogous to weather (e.g., Zhao *et al.* 2001). This should be obvious by consideration of the difference between the effects of kG magnetic fields in solar-type and Ap stars. By way of speculation, we would hypothesize that the circulation sweeps the spots produced by any dynamo in the more massive star off its face onto its less massive companion where they are subducted by the flow and their magnetic field redistributed. This mechanism provides a possible source of the ephemeral dark spots often invoked to explain peculiarities of

W UMa-type light curves, as we have done here. The inevitable random variations in the distribution of spots being carried along by the circulation would still give measurable temporary concentrations of spots.

Perhaps the most important upshot here is that there are limits to just how precisely we can know the physical properties of a contact binary from light curve solutions. Our fits show that the mass ratio, for instance, seems to be uncertain by up to 9% (the range of values in columns 4–6 in Table 3). This is in contrast to the tenths of a percent derived as formal errors of a typical fit. It also echos Popper's (1984) reasoning in arguing that such formal errors are misleading, that they underestimate the true uncertainties by about a factor of three. This result is unfortunate, since it limits our ability to define changes in physical properties, most notably the fillout, that might be related to fluctuations of the energy-transfer mechanism.

6. Acknowledgements

References

Alton, K. B., and Stępień, K. 2018, *Acta. Astron.*, **68**, 449.

Barnes, J. R., Lister, T. A., Hilditch, R. W., and Collier Cameron, A. 2004, *Mon. Not. Roy. Astron. Soc.*, **348**, 1321.

Chen, W. P., Sanchawala, K., and Chiu, M. C. 2006, *Astron. J.*, **131**, 990.

Diethelm, R. 2010, *Inf. Bull. Var. Stars*, No. 5945, 1.

Diethelm, R. 2011, *Inf. Bull. Var. Stars*, No. 5992, 1.

Diethelm, R. 2012, *Inf. Bull. Var. Stars*, No. 6011, 1.

Eaton, J. A. 1986, *Acta. Astron.*, **36**, 79.

Eaton, J. A., Henry, G. W., and Fekel, F. C. 1996, *Astrophys. J.*, **462**, 888.

Eaton, J. A., Odell, A. P., and Nitschelm, C. 2020, *Mon. Not. Roy. Astron. Soc.*, in press.

Eaton, J. A., Wu, C.-C., and Ruciński, S. M. 1980, *Astrophys. J.*, **239**, 919.

Lucy, L. B. 1967, *Z. Astrophys.*, **65**, 89.

Lucy L. B. 1968, *Astrophys. J.*, **151**, 1123.

Nagai, K. 2018, *Bull. Var. Star Obs. League Japan*, No. 64, 1.

Nagai, K. 2019, *Bull. Var. Star Obs. League Japan*, No. 66, 1.

Pepper, J., *et al.* 2007, *Publ. Astron. Soc. Pacific*, **119**, 923.

Pilecki, B., and Stępień, K. 2012, *Inf. Bull. Var. Stars*, No. 6012, 1.

Pojmański, G. 1997, *Acta. Astron.*, **47**, 467.

Popper, D. M. 1984, *Astron. J.*, **89**, 132.

Pribulla T., Chochol, D., Rovithis, P., and Rovithis-Livanou, H. 1997, *Inf. Bull. Var. Stars*, No. 4435, 1.

Ruciński, S. M. 1969, *Acta Astron.*, **19**, 245.

Ruciński, S. M., and Paczynski, B. 2002, *Inf. Bull. Var. Stars*, No. 5321, 1.

Ruciński, S. M., and Vilhu, O. 1983, *Mon. Not. Roy. Astron. Soc.*, **202**, 1221.

Ruciński, S. M., Vilhu, O., and Whelan, J. A. J. 1985, *Astron. Astrophys.*, **143**, 153.

Rukmini, J., and Shanti Priya, D. 2016, *J. Chem. Biol. Phys. Sci.*, **6**, 926.

Samec, R. G., Labadorf, C. M., Hawkins, N. C., Faulkner, D. R., and Van Hamme, W. 2011, *Astron. J.*, **142**, 117.

Samec, R. G., Melton, R. A., Figg, E. R., Labadorf, C. M., Martin, K. P., Chamberlain, H. A., Faulkner, D. R., and van Hamme, W. 2010, *Astron. J.*, 140, 1150.

Shanti Priya, D. Sriram, K., and Vivekananda Rao, P. 2013, *Res. Astron. Astrophys.*, **13**, 465.

Stępień, K. 2009, *Mon. Not. Roy. Astron. Soc.*, **397**, 857.

Stępień, K., Schmitt, J. H. M. M., and Voges, W. 2001, *Astron. Astrophys.*, **370**, 157.

University of Arizona. 2006, 2007, 2008, 2009, Catalina Sky Survey (http://www.lpl.arizona.edu/css).

van Hamme, W. 1993, *Astron. J.*, **106**, 2096.

Wilson, R. E. 1990, *Astrophys. J.*, **356**, 613.

Wilson, R. E. 1994, *Publ. Astron. Soc. Pacific*, **106**, 921.

Wilson, R. E., and Devinney, E. J. 1971, *Astrophys. J.*, **166**, 605.

Wilson, R. E., and van Hamme, W. 2015, *Computing Binary Star Observables*, privately published manual, U. Florida web site.

Wozniak, P. R., *et al.* 2004, *Astron. J.*, **127**, 2436.

Zhao, J., Kosovichev, A. G., and Duvall, T. L., Jr. 2001, *Astrophys. J.*, **557**, 384.